

Endocytosed dsRNAs induce lysosomal membrane permeabilization that allows cytosolic dsRNA translocation for *Drosophila* RNAi responses

Received: 27 June 2022

Accepted: 2 August 2024

Published online: 14 August 2024

 Check for updates

Tsubasa Tanaka^{1,2}, Tamaki Yano³, Shingo Usuki⁴, Yoko Seo^{1,5}, Kento Mizuta^{1,5}, Maho Okaguchi^{1,5}, Maki Yamaguchi^{1,5}, Kazuko Hanyu-Nakamura¹, Noriko Toyama-Sorimachi⁶, Katja Brückner^{7,8} & Akira Nakamura^{1,2}✉

RNA interference (RNAi) is a gene-silencing mechanism triggered by the cytosolic entry of double-stranded RNAs (dsRNAs). Many animal cells internalize extracellular dsRNAs via endocytosis for RNAi induction. However, it is not clear how the endocytosed dsRNAs are translocated into the cytosol across the endo/lysosomal membrane. Herein, we show that in *Drosophila* S2 cells, endocytosed dsRNAs induce lysosomal membrane permeabilization (LMP) that allows cytosolic dsRNA translocation. LMP mediated by dsRNAs requires the lysosomal Cl⁻/H⁺ antiporter ClC-b/DmOstm1. In *clc-b* or *dmostm1* knockout S2 cells, extracellular dsRNAs are endocytosed and reach the lysosomes normally but fail to enter the cytosol. Pharmacological induction of LMP restores extracellular dsRNA-directed RNAi in *clc-b* or *dmostm1*-knockout cells. Furthermore, *clc-b* or *dmostm1* mutant flies are defective in extracellular dsRNA-directed RNAi and its associated antiviral immunity. Therefore, endocytosed dsRNAs have an intrinsic ability to induce ClC-b/DmOstm1-dependent LMP that allows cytosolic dsRNA translocation for RNAi responses in *Drosophila* cells.

RNA interference (RNAi) is an evolutionarily conserved gene-silencing mechanism induced by double-stranded RNAs (dsRNAs). RNAi is triggered by the entry of dsRNAs into the cytosol, where the RNAi machinery and target mRNAs primarily reside¹. Cytosolic dsRNAs are processed into ~21-nucleotide small interference RNAs (siRNAs), which are subsequently incorporated into the RNAi effector, called RNA-induced silencing complex (RISC). Many animal cells naturally take up exogenous naked dsRNAs via endocytosis for RNAi induction^{2,3}. This

phenomenon has been widely used in genetic screening as soaking RNAi. The endocytosed dsRNAs should be translocated to the cytosol in order to trigger RNAi. Thus far, the only known channel for dsRNA translocation is SID-1 in *Caenorhabditis elegans*. Cell surface SID-1 imports extracellular dsRNAs into the cytosol and promotes systemic RNAi spreading^{2,3}. Although the precise function of SID-1 on endo/lysosomes remains unclear, two mouse SID-1 homologs, SIDT1 and SIDT2, appear to mediate the cytosolic translocation of intravesicular dsRNAs to elicit

¹Department of Germline Development, Institute of Molecular Embryology and Genetics, Kumamoto University, Kumamoto, Japan. ²Graduate School of Pharmaceutical Sciences, Kumamoto University, Kumamoto, Japan. ³Graduate School of Pharmaceutical Sciences, Tohoku University, Sendai, Japan. ⁴Liaison Laboratory Research Promotion Center, Institute of Molecular Embryology and Genetics, Kumamoto University, Kumamoto, Japan. ⁵School of Pharmacy, Kumamoto University, Kumamoto, Japan. ⁶Division of Human Immunology, International Research and Development Center for Vaccines, The Institute of Medical Science, The University of Tokyo (IMSUT), Tokyo, Japan. ⁷Department of Cell and Tissue Biology, University of California San Francisco, San Francisco, CA, USA. ⁸Deceased: Katja Brückner. ✉e-mail: akiran@kumamoto-u.ac.jp

immune responses^{4,5}. However, SID-1 homologs are dispensable for systemic RNAi in several other species³ and are even absent in dipteran insects, including *Drosophila*². Thus, dsRNAs are translocated across the membrane in these species through a hitherto unknown mechanism. Herein, we report that in *Drosophila* cells, lysosomal membrane permeabilization (LMP) underlies the cytosolic translocation of intravesicular dsRNAs to induce RNAi.

Results

Drosophila CIC-b and Ostm1 are required for soaking RNAi

CIC-b and CG14969 were identified from a genome-wide knockdown (KD) screen in cultured *Drosophila* Kc cells as suppressors of the cell-death phenotype under PDGF/VEGF receptor (PVR)-KD conditions (Supplementary Fig. 1a)⁶. In this screen, Kc cells were cultured with mixtures of dsRNAs targeting *pvr* and each specific gene. Unexpectedly, we found that under the same conditions, *pvr* KD was impaired in CIC-b- and CG14969-depleted cells (Supplementary Fig. 1b). To examine whether CIC-b and CG14969 are factors involved in RNAi, we generated *clc-b* and *CG14969* knockout (KO) cell lines from hemocyte-like S2 cells (Supplementary Figs. 2 and 3). These KO cells were transfected with firefly luciferase (*fluc*)-expressing plasmids and then cultured in the media containing *fluc* dsRNAs (*dsfluc*) of various lengths (139, 259, 555, and 1006 bp) to induce RNAi (Fig. 1a). *dsfluc* treatment resulted in the marked reduction of *fluc* mRNA levels in control S2 cells, although its efficacy slightly varied among *dsfluc* lengths (Fig. 1b)⁷. In contrast, *fluc* mRNA levels in *clc-b* or *CG14969* KO cells treated with *dsfluc* of any length remained comparable to those in untreated cells (Fig. 1b). Therefore, CIC-b and CG14969 are required for extracellular dsRNA-directed RNAi.

CIC-b and CG14969 are homologs of mammalian CIC-7 and Ostm1, respectively (hereinafter CG14969 is referred to as DmOstm1). CIC-7 forms a complex with its β -subunit Ostm1. The CIC-7/Ostm1 complex functions as a lysosomal $2\text{Cl}^-/\text{H}^+$ antiporter that couples the influx of two chloride ions to the efflux of a single proton⁸. We found that CIC-b and DmOstm1 co-localized on vesicular structures in S2 cells (Fig. 1c, d). GFP-tagged CIC-b (CIC-b-GFP) was mostly overlapping with the lysosomal marker Lamp1 tagged with tdTomato (Lamp1-tdTom) and to a lesser degree, with the late endosomal and lysosomal marker Rab7 (Fig. 1c, d). In contrast, the subcellular distribution of CIC-b-GFP was distinct from that of the early endosomal marker Rab5 or the recycling endosomal marker Rab11 (Fig. 1c, d). We also found that endogenous CIC-b was co-immunoprecipitated with DmOstm1 in S2 cell lysates (Fig. 1e), which is consistent with the CIC-7-Ostm1 interaction in mouse brain lysates⁹. These results suggest that CIC-b and DmOstm1 form a complex preferentially on lysosomes, similar to their mammalian homologs.

CIC-b/Ostm1 is required for soaking RNAi in vivo

To assess the in vivo requirements of CIC-b and DmOstm1 for RNAi, we generated null mutant flies for *clc-b* and *dmostm1* (Supplementary Fig. 4) and examined the effect on extracellular dsRNA-directed RNAi in hemocytes, which can internalize exogenously applied dsRNAs via endocytosis². Extracellular dsRNA-directed RNAi was induced by injecting *GFP* dsRNAs (*dsGFP*) into the body cavity of adult females expressing *GFP* specifically in the hemocytes. The injection of *dsGFP* significantly reduced the *GFP* mRNA levels in wild-type flies but had almost no effect on *clc-b*^{-/-} and *dmostm1*^{-/-} flies (Fig. 2a). These results indicate that extracellular dsRNA-directed RNAi requires CIC-b and DmOstm1 in *Drosophila* hemocytes in vivo and in cultured cells.

CIC-b/Ostm1 is required for antiviral immunity

RNAi is responsible for antiviral defense in *Drosophila*¹⁰. Upon virus infection, dsRNAs from replicating viral genome are processed into siRNAs, which play roles in limiting and controlling virus infection¹⁰. RNAi-mediated antiviral response also systemically spreads, although

the underlying mechanisms remain to be solved¹⁰⁻¹². We examined the effect of the loss of CIC-b or DmOstm1 on the susceptibility to *Drosophila* C virus (DCV), a positive-sense single-stranded RNA virus¹³. Upon infection with DCV, *clc-b*^{-/-} and *dmostm1*^{-/-} flies had a significantly lower survival rate than wild-type flies (Fig. 2b). DCV-infected *clc-b*^{-/-} and *dmostm1*^{-/-} flies had a median survival of 5 days, which was shorter than that of wild-type flies (>7 days). The mortality in DCV-infected mutant flies was positively correlated with viral RNA levels (Fig. 2c). At day 3 post-infection, the DCV RNA levels in *clc-b*^{-/-} or *dmostm1*^{-/-} flies were ~10- or 5.7-fold higher than those in wild-type flies, respectively. Notably, more viral RNAs accumulated in *clc-b*^{-/-} flies than in *dmostm1*^{-/-} flies. Furthermore, while flies lacking *clc-b* could not be maintained as homozygous stocks, *dmostm1*^{-/-} flies could be maintained across generations. These results suggest that the CIC-b functions were not completely dependent on DmOstm1 in vivo. Supporting this idea, the structural study of the vertebrate homologs has shown that the CLC-7 subunit constitutes the multimembrane-spanning Cl^-/H^+ antiporter, whereas OSTM1 covers the luminal surface of CLC-7 and has a minor role in the conformation of the ion-conduction pathway. OSTM1 is proposed to protect CLC-7 from the degradative environment of the lysosomal lumen and contribute a regulatory role¹⁴. The results nevertheless suggest that CIC-b and DmOstm1 are required for RNAi-associated antiviral responses.

To examine whether the increased susceptibility against DCV infection in *clc-b*^{-/-} and *dmostm1*^{-/-} flies was due to a failure of RNAi response in infected cells, Ago2, the catalytic subunit of the siRNA-RISC¹, was immunopurified from whole fly lysates and co-purified siRNAs were subjected to deep sequencing. We found that, even in *clc-b*^{-/-} or *dmostm1*^{-/-} flies, siRNAs targeting the DCV genome were produced in DCV-injected flies (Fig. 2d). These results indicate that the processing of viral RNA into siRNAs and their loading into the Ago2-RISCs in infected cells occur even in the absence of CIC-b or DmOstm1. Although the relative levels of DCV-derived siRNAs in *clc-b*^{-/-} or *dmostm1*^{-/-} flies were 50-130-fold higher than that in wild-type flies (Fig. 2d), the deficiency of the lysosomal Cl^-/H^+ antiporter resulted in increased susceptibility against DCV infection (Fig. 2b, c). Therefore, RNAi-independent antiviral responses and/or cell non-autonomous antiviral RNAi responses, such as systemic RNAi spread^{11,12}, appear to be impaired in *clc-b*^{-/-} and *dmostm1*^{-/-} flies.

We next examined RNAi from dsRNAs transcribed in the nucleus of *clc-b* and *dmostm1* mutant flies. When *GFP* and *dsGFP* were specifically co-expressed in the hemocytes, the *GFP* mRNA levels were similarly reduced in wild-type, *clc-b*^{-/-}, and *dmostm1*^{-/-} flies but not in RNAi-defective *dicer-2*^{-/-} (*dcr-2*^{-/-}) flies (Fig. 2e). Similarly, nuclear expression of hairpin dsRNAs against *white*, a gene responsible for eye pigmentation, caused a pale eye color in the wild-type, *clc-b*^{-/-}, and *dmostm1*^{-/-} flies (Fig. 2f). In contrast, expression of *white* dsRNAs did not affect the eye color of *dcr-2*^{-/-} and *ago2*^{-/-} flies (Fig. 2f), as reported previously^{15,16}. These results indicate that dsRNAs expressed in the nucleus efficiently induce RNAi even in cells lacking CIC-b or DmOstm1. As nuclear and extracellular dsRNAs function in the same pathway to induce RNAi after they reach the cytosol, it is likely that CIC-b and DmOstm1 are involved in the pathway that leads to the cytosolic translocation of extracellular dsRNAs.

CIC-b/Ostm1 is dispensable for dsRNA internalization

To examine whether CIC-b and DmOstm1 are required for internalization and subsequent vesicular trafficking of dsRNAs, intracellular dsRNAs were visualized using FITC-labeled *dsfluc*, which was fully capable of inducing RNAi in S2 cells (Supplementary Fig. 5). After a 2 or 24 h of incubation with FITC-*dsfluc*-containing medium, the signal intensity of intracellular FITC in *clc-b* or *dmostm1* KO cells was comparable with that of control S2 cells (Fig. 3a, b). ~30% of the FITC signals overlapped with Lamp1-tdTom in control S2 cells cultured in FITC-*dsfluc*-containing medium for 2 h, and this percentage increased up to

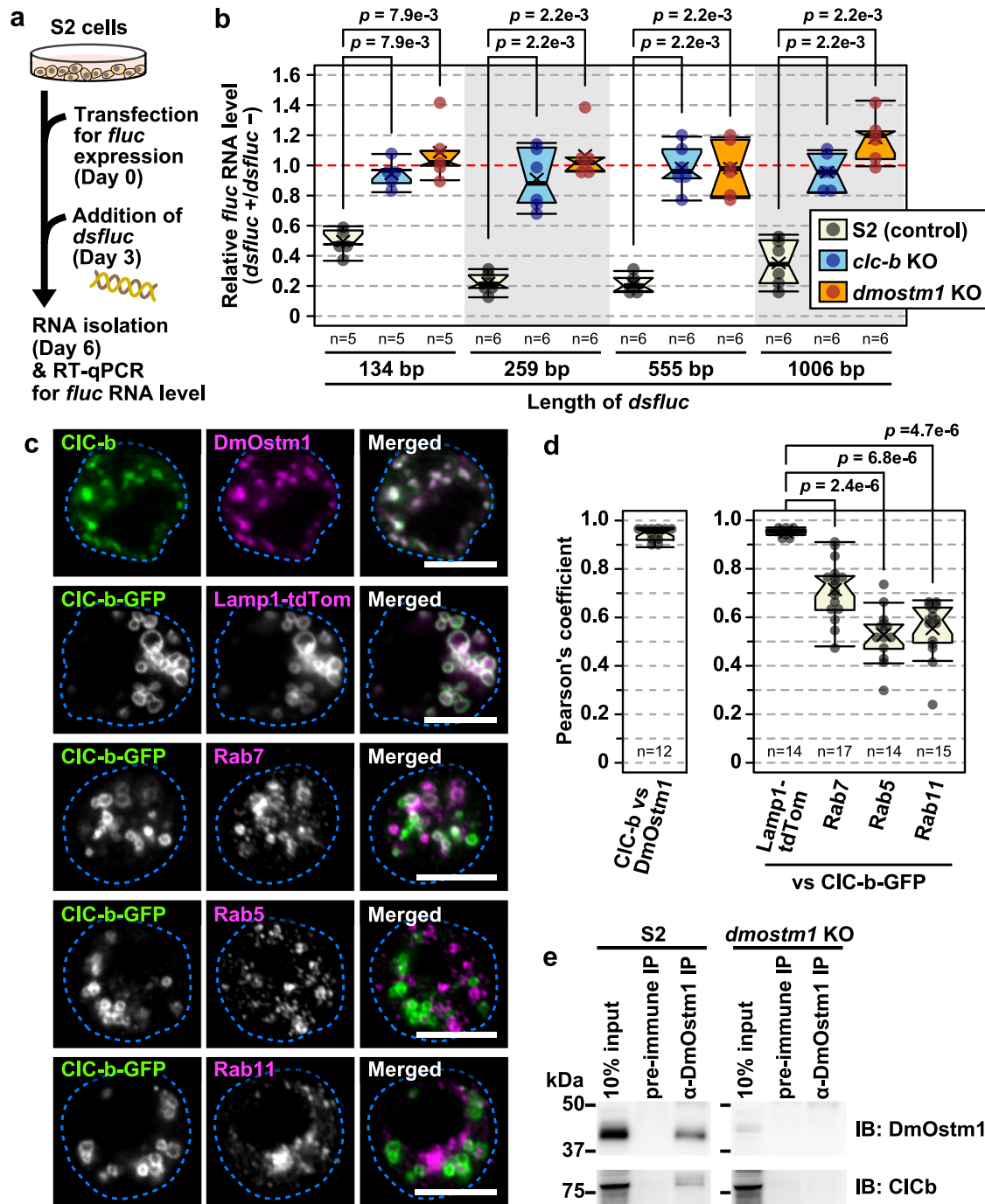


Fig. 1 | The lysosomal Cl⁻/H⁺ antiporter CIC-b/DmOstm1 is required for extra-cellular dsRNA-directed RNAi in *Drosophila* S2 cells. **a A schematic diagram of experiments to evaluate the *fluc* mRNA levels in S2 cells. **b** The relative *fluc* mRNA levels determined by RT-qPCR in control, *clc-b*, and *CG14969* KO S2 cells. Cells were co-transfected with *fluc*- and *Renilla luciferase* (*Rluc*)-expressing plasmids and were then cultured with *dsfluc* of different lengths (139, 259, 555, and 1006 bp). The *fluc* mRNA levels were normalized to *Rluc* mRNA levels. The number of samples analyzed (*n*) is indicated in the graphs. The normalized *fluc* mRNA levels in *dsfluc*-untreated cells were arbitrarily defined as 1. *P*-values were calculated using two-sided Mann-Whitney U test. **c** Localization of CIC-b and DmOstm1, or CIC-b-GFP and either lysosomal marker Lamp1-tdTom, the late endosomal and lysosomal marker Rab7, the early endosomal marker Rab5, or the recycling endosomal marker Rab11. Cells are outlined by blue dashed lines. Scale bars: 5 μ m. **d** Pearson's**

coefficients between CIC-b and DmOstm1 (left), or CIC-b-GFP and endo/lysosomal markers (Lamp1-tdTom, Rab7, Rab5, and Rab11) (right). The number of samples (*n*) used to calculate Pearson's coefficients is indicated in the graph. *P*-values were calculated using two-sided Mann-Whitney U test. **e** Co-immunoprecipitation of CIC-b with DmOstm1. S2 or *dmostm1* KO cell lysates were immunoprecipitated with rat anti-DmOstm1 or pre-immune sera, and then immunoblotted with rabbit anti-CIC-b and rabbit anti-DmOstm1 antisera. The data were reproducible among three independent immunoprecipitation experiments. All box plots indicate the median (center line), the mean (\times), the interquartile range (IQR) between the first and third quartile (Q1 and Q3; box), 1.5 \times IQR above Q1 and below Q3 (whiskers), and each data point (dots). Statistics source data and uncropped blots for Fig. 1 are provided in the Source Data file.

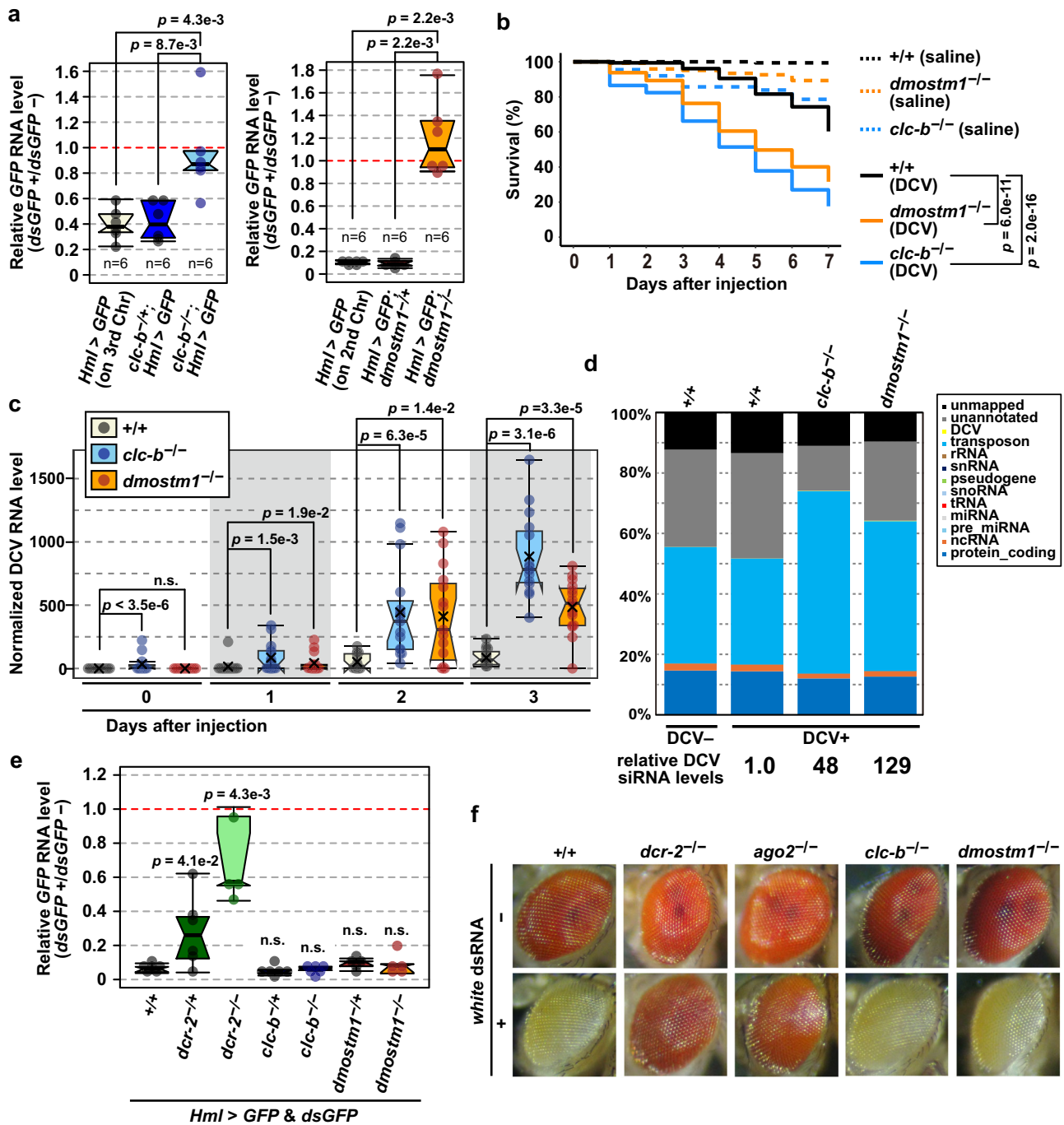


Fig. 2 | CIC-b and DmOstm1 are required for extracellular dsRNA-directed RNAi and antiviral immunity in vivo. **a** The relative *GFP* mRNA levels determined by RT-qPCR in *dsGFP*-injected flies expressing *GFP* under the control of hemocyte-specific *Hml* Gal4 drivers. The number of independent experiments is indicated in the graph. The *GFP* mRNA levels in PBS-injected flies were arbitrarily defined as 1. *P*-values were calculated using two-sided Mann–Whitney U test. **b** Survival rates of DCV- or saline-injected flies. The day of injection was designated as day 0. At least 5 independent experiments (totally > 100 flies) were conducted in each condition. *P*-values were calculated using log-rank test. **c** The normalized DCV RNA levels determined by RT-qPCR in DCV-injected flies. Ten flies were injected in each experiment and 15 independent experiments were conducted in each time point. *P*-values were calculated using two-sided Mann–Whitney U test. n.s.: not significant ($p > 0.05$). **d** Annotation of Ago2-associated small RNAs. rRNA, ribosomal RNA; snRNA, small nuclear RNA; snoRNA, small nucleolar RNA, tRNA, transfer RNA;

miRNA, microRNA; ncRNA, noncoding RNA. The DCV-derived siRNA reads were normalized to the total siRNA reads, and the relative abundance of DCV sequence reads over DCV RNA level are shown at the bottom of the graph. **e** The relative *GFP* mRNA levels in flies co-expressing *GFP* and *dsGFP* specifically in hemocytes. At least 5 independent experiments were conducted in each genotype. The *GFP* mRNA levels in flies expressing *GFP* alone were arbitrarily defined as 1. *P*-values between the wild-type and each genotype were calculated using two-sided Mann–Whitney U test. n.s.: not significant ($p > 0.05$). **f** Eye colors of flies of different genotypes with or without *GMR-wIR* expression. All box plots indicate the median (center line), the mean (×), the interquartile range (IQR) between the first and third quartile (Q1 and Q3; box), 1.5× IQR above Q1 and below Q3 (whiskers), and each data point (dots). Full genotypes of fly lines are shown in Supplementary Table 1. Statistics source data tested for Fig. 2 are provided in the Source Data file.

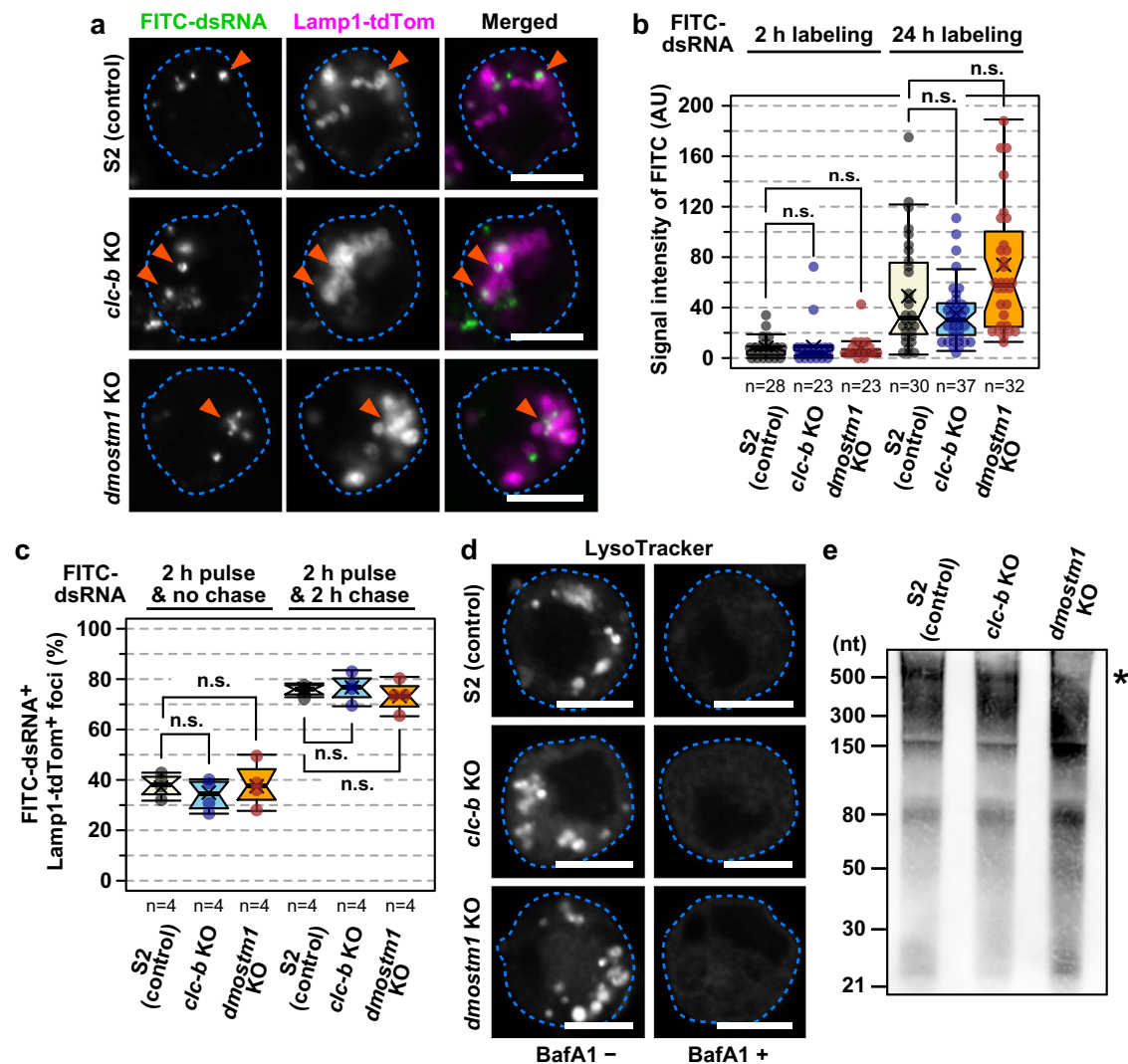


Fig. 3 | CIC-b and DmOstm1 are dispensable for internalization and vesicular trafficking of extracellular dsRNAs. **a** FITC-dsRNAs and Lamp1-tdTom in control, *clc-b*, and *dmostm1* KO S2 cells treated with FITC-dsRNAs for 2 h. FITC-dsRNA⁺ Lamp1-tdTom⁺ foci are indicated by arrowheads. **b** FITC intensity within cells treated with FITC-dsRNAs for 2 or 24 h. The number of cells (n) examined is indicated in the graph. AU: arbitrary units. **c** The percentage of FITC-dsRNA⁺ Lamp1-tdTom⁺ foci in cells that were chased for 0 or 2 h after 2-h pulse-labeling with FITC-dsRNAs. The number of independent experiments is indicated in the graph. **d** Images for LysoTracker in control, *clc-b*, and *dmostm1* KO S2 cells that were pretreated with or without a v-ATPase inhibitor, bafilomycin A1 (BafA1). The data

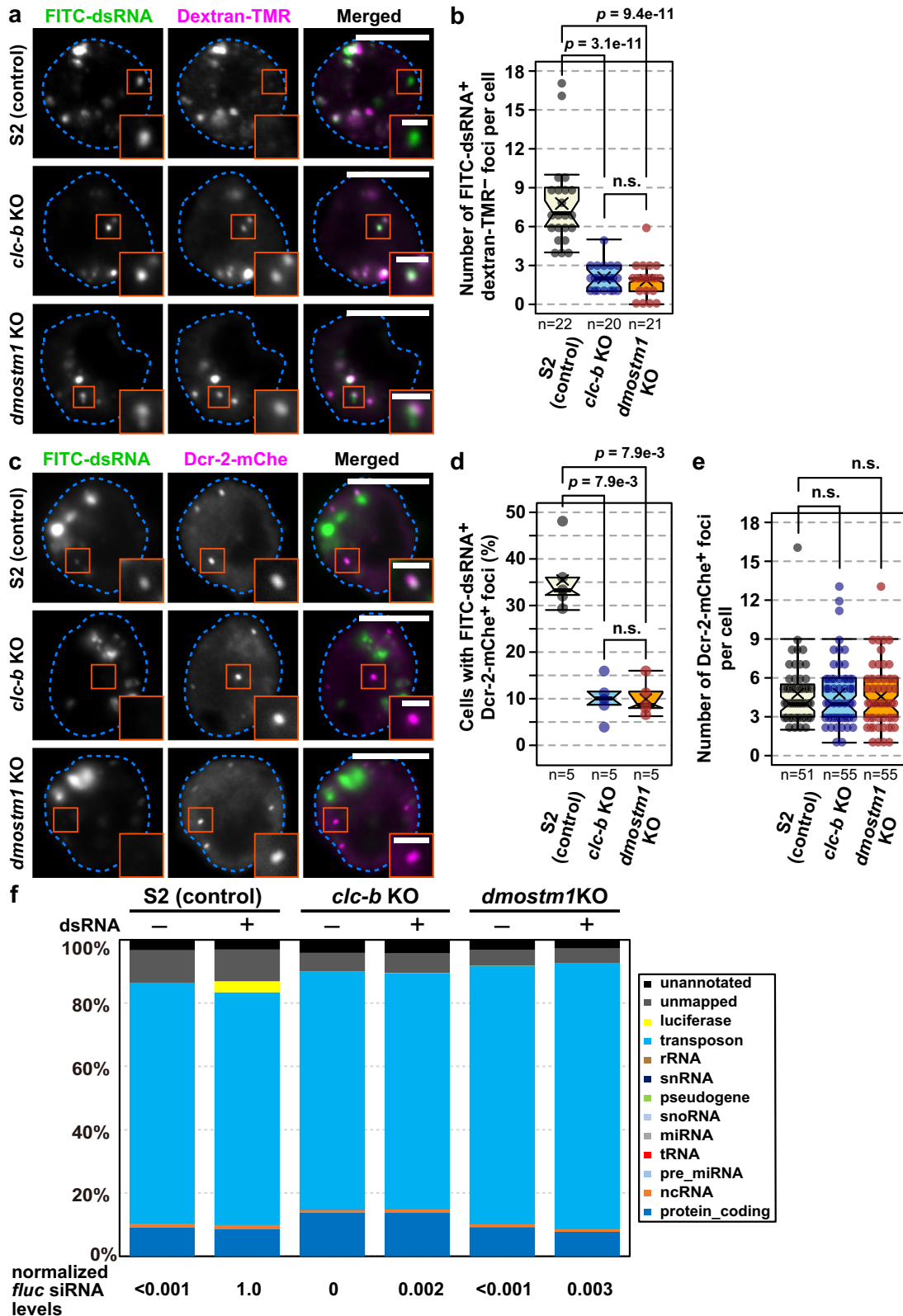
were reproducible among two independent experiments. **e** Biotin-RNAs isolated from biotin-*dsfluc*-treated cells. The position of the intact biotin-RNA is marked with an asterisk. The data were reproducible among two independent experiments. For **a** and **d** cells are outlined by blue dashed lines. Scale bars: 5 μ m. For **b** and **c** p-values were calculated using two-sided Mann-Whitney U test. n.s. not significant ($p > 0.05$). All box plots indicate the median (center line), the mean (\times), the interquartile range (IQR) between the first and third quartile (Q1 and Q3; box), 1.5 \times IQR above Q1 and below Q3 (whiskers), and each data point (dots). Statistics source data tested for Fig. 3 are provided in the Source Data file.

-75% when the pulse was followed by a 2-hour chase (Fig. 3a, c). These findings indicate that endocytosed dsRNAs were targeted to the lysosomes. The percentage of FITC-*dsfluc*⁺ Lamp1-tdTom⁺ foci remained unchanged in *clc-b* or *dmostm1* KO cells (Fig. 3a, c). Thus, CIC-b and DmOstm1 are dispensable for internalization and the subsequent lysosomal targeting of dsRNAs.

Intravesicular chloride ions have been shown to assist the activity of the proton pump vacuolar H⁺-ATPase (v-ATPase) that promotes endo/lysosomal acidification⁸. Given that v-ATPase is required for extracellular dsRNA-directed RNAi⁷, the RNAi defects in *clc-b* or *dmostm1* KO cells might be attributed to the impaired v-ATPase activity. However, this was unlikely because, similar to cultured neurons and fibroblasts from *CIC-7* and *ostm1* KO mice⁸, both *clc-b* and *dmostm1* KO cells were not defective in v-ATPase-dependent vesicular acidification assessed using a pH-sensitive LysoTracker dye (Fig. 3d).

Endocytosed macromolecules are generally digested by lysosomal enzymes. We examined whether CIC-b and DmOstm1 are implicated in RNAi by regulating dsRNA degradation. To evaluate dsRNA degradation, we cultured cells with RNAi-inducible biotin-labeled *dsfluc* (Supplementary Fig. 5). Biotinylated-RNAs isolated from control, *clc-b*, and *dmostm1* S2 KO cells showed a similar electrophoretic pattern characterized by multiple smeared bands that were smaller than intact biotinylated-RNAs (Fig. 3e). These results suggest that dsRNA degradation occurs after endocytosis and is independent of CIC-b and DmOstm1.

The formation of cytosolic dsRNA foci depends on CIC-b/Ostm1
We next examined whether the cytosolic translocation of endocytosed dsRNAs depends on CIC-b and DmOstm1. To distinguish intravesicular dsRNAs from cytosolic dsRNAs in situ, a culture medium containing FITC-dsRNAs was supplemented with dextran-



tetramethylrhodamine (TMR), which is nonspecifically endocytosed and labels entire endo/lysosomes. Thus, intravesicular FITC-dsRNA signals are positive for dextran-TMR. Interestingly, a few FITC foci (mostly less than 10 per cell) were negative for dextran-TMR in control S2 cells, and the number of these FITC⁺ TMR⁻ foci per cell was markedly decreased in *clc-b* or *dmostm1* KO cells (Fig. 4a, b).

CIC-b/Ostm1-dependent incorporation of siRNAs into the RISC
 We also examined the co-localization of endocytosed FITC-dsRNAs with the dsRNA processing enzyme Dcr-2 and its cofactor R2D2. The Dcr-2/R2D2 complex forms cytosolic foci that are proposed to be the sites for the assembly of the RISC¹⁷. When Dcr-2-mCherry (mCherry)-expressing cells were cultured with FITC-dsRNAs for 24 h, ~35% of the control S2 cells had one or two foci that were double positive for FITC

Fig. 4 | Formation of cytosolic dsRNA foci and incorporation of extracellular dsRNA derived siRNA into the Ago2-complex depend on CIC-b and DmOstm1. **a** Representative images of FITC-dsRNA and dextran-TMR in control, *clc-b*, and *dmostm1* KO S2 cells. Cells were cultured with 1 $\mu\text{g}/\text{mL}$ FITC-dsRNAs and 100 $\mu\text{g}/\text{mL}$ dextran-TMR for 24 h. High-magnification views of the bracketed area are shown at the lower right of each panel. **b** The number of FITC-dsRNA foci negative for dextran-TMR per cell. The number of cells (n) examined is indicated in the graph. **c** Representative images of FITC-dsRNAs and Dcr-2-mChe in control, *clc-b*, and *dmostm1* KO S2 cells. Cells expressing Dcr-2-mChe were cultured with FITC-dsRNAs for 24 h. High-magnification views of the bracketed area are shown at the lower right of each panel. **d** The percentage of the control, *clc-b*, or *dmostm1* KO S2 cells with FITC-dsRNA foci overlapping with Dcr-2-mChe. The number of independent experiments (n) is indicated in the graph. **e** The number of Dcr-2-mChe⁺ foci in the

Dcr-2-mChe-expressing cells treated with FITC-dsRNAs. The number of cells (n) examined is indicated in the graph. **f** Annotation of Ago2-associated small RNAs. rRNA, ribosomal RNA; snRNA, small nuclear RNA; snoRNA small nucleolar RNA; tRNA, transfer RNA; miRNA, microRNA; ncRNA, noncoding RNA. The normalized abundance of DCV sequence reads against transposon sequence reads was shown at the bottom of the graph. For **a** and **c**, cells are outlined by blue dashed lines. Scale bars: 5 μm or 1 μm (lower right insets). For **b**, **d**, and **e**, p -values were calculated using two-sided Mann–Whitney U test. n.s.: not significant ($p > 0.05$). All box plots indicate the median (center line), the mean (\times), the interquartile range (IQR) between the first and third quartile (Q1 and Q3; box), $1.5 \times \text{IQR}$ above Q1 and below Q3 (whiskers), and each data point (dots). Statistics source data tested for Fig. 4 are provided in the Source Data file.

and mChe (Fig. 4c, d). In contrast, less than 10% of the *clc-b* or *dmostm1* KO cells exhibited double positive foci, despite a comparable number of Dcr-2-mChe⁺ foci per cell (Fig. 4c–e). Similar results were obtained for R2D2 tagged with mScarlet (mSca-R2D2) (Supplementary Fig. 6). Thus, *clc-b* or *dmostm1* KO cells failed to form cytosolic dsRNA foci, most likely because of the impaired translocation of endocytosed dsRNAs into the cytosol.

To examine whether endocytosed extracellular dsRNAs are processed to siRNAs and incorporated in the Ago2-containing RISC complex, we immunopurified Ago2 from S2, *clc-b*, or *dmostm1* KO cells and copurified RNAs are deep-sequenced (Fig. 4f). In the absence of extracellular dsRNA administration, the majority of small RNAs copurified with Ago2 matched to transposon sequence as reported¹⁸. When cells were cultured for 40 h with *fluc* dsRNAs in the medium, siRNAs that matched to the *fluc* sequence were detected in the immunopurified Ago2-containing complex in S2 cells (Fig. 4f). However, in *clc-b* or *dmostm1* KO cells, the percentage of extracellular dsRNA-derived siRNAs in the Ago2-containing complex was reduced by a factor of 300–400 (Fig. 4f). The proportion of other siRNA profiles for the *Drosophila* transposons and genomic genes did not change between with and without dsRNA administrations. These results indicate that, in *clc-b* or *dmostm1* KO cells, extracellular dsRNA-derived siRNAs were not loaded into the Ago2-RISC, further supporting the idea that the lysosomal Cl⁻/H⁺ antiporter is crucial for the release of endocytosed dsRNA into the cytosol.

CIC-b/Ostm1 promotes dsRNA-induced LMP

Lysosomal contents can be released into the cytosol via destabilization of the lysosomal membrane, referred to as lysosomal membrane permeabilization (LMP). As LMP can be induced by lysosomal accumulation of ionic molecules¹⁹, we hypothesized that the anionic polymers, dsRNAs, induce LMP, subsequently leading to their cytosolic release. LMP was assessed by examining the relocation of a β -galactoside-binding lectin, Galectin¹⁹. Galectin usually exhibits diffused localization in the cytosol but accumulates in permeabilized endo/lysosomes because of cytosolic exposure of luminal glycans. Treatment of cells with an LMP-inducer, chloroquine (CQ), increased the number of mSca-Galectin⁺ foci -5-fold compared with that in untreated cells, and most of the mSca⁺ foci overlapped with CIC-b signals (Supplementary Fig. 7). These results show that similar to that in mammalian cells, Galectin serves as a specific marker for LMP in *Drosophila* cells.

We found that FITC-dsRNA-treated S2 cells had a significantly increased number of mSca-Galectin⁺ foci when compared with untreated cells (Figs. 5a, b, Supplementary Fig. 8). These mSca-Galectin⁺ foci overlapped with CIC-b, DmOstm1, and to a lesser degree, with Rab7, but not with Rab5 or Rab11 (Fig. 5c, d). In contrast, in *clc-b* or *dmostm1* KO cells, dsRNA treatment had no effect on the number of mSca-Galectin⁺ foci (Fig. 5a, b, Supplementary Fig. 8), even though extracellular dsRNAs were endocytosed and reached the lysosomes normally (Fig. 3a–c). Correspondingly, the number of FITC and mSca-double positive foci in *clc-b* or *dmostm1* KO cells was significantly lower

than that in control S2 cells (Fig. 5e). These results indicate that endocytosed dsRNAs induce LMP in a CIC-b/DmOstm1-dependent manner.

LMP mediated by dsRNAs in *clc-b* KO cells was fully restored by expression of GFP-tagged CIC-b, but not mutated CIC-b with an alanine substitution for the conserved glutamate residue (E340A) that is critical for the transporter activity of mouse CIC-7 (Fig. 6a, b)²⁰. Full restoration of dsRNA-mediated LMP of *clc-b* KO cells was also achieved upon co-expression of mouse Ostm1 and GFP-tagged mouse CIC-7 (CIC-7-GFP), but not its ion transport-defective form, CIC-7 (E312A)-GFP (Fig. 6a, b). The results suggest that dsRNA-mediated LMP depends on chloride ion regulation in the lysosomes via the evolutionarily conserved Cl⁻/H⁺ antiporter.

We further examined whether pharmacological induction of LMP restores extracellular dsRNA-directed RNAi in *clc-b* or *dmostm1* KO cells. Two LMP inducers, CQ and L-leucyl-L-leucine methyl ester (LLME), effectively induced LMP in *clc-b* or *dmostm1* KO cells as in control S2 cells (Supplementary Fig. 9). Intriguingly, the treatment with the LMP inducers restored *fluc* RNAi in *clc-b* and *dmostm1* KO cells (Fig. 6c, d). Overall, the results suggest that CIC-b and DmOstm1 promote dsRNA-mediated LMP that allows cytosolic dsRNA translocation to induce RNAi.

Discussion

The translocation of endo/lysosomal contents to the cytosol has diverse effects on cell activities. The cytosolic translocation of intravesicular dsRNAs elicits RNAi responses in various animal cells^{2,3}. Despite the importance of RNAi processes, the mechanism underlying the cytosolic dsRNA translocation has remained unknown. In this study, we showed that in *Drosophila* S2 cells, endocytosed dsRNAs induced LMP that allowed the translocation of dsRNAs themselves to the cytosol. We also showed that dsRNA-mediated LMP required the lysosomal Cl⁻/H⁺ antiporter CIC-b/DmOstm1, which was critical for RNAi and antiviral responses.

The CIC family proteins are involved in the endo/lysosomal functions⁸. In mammalian cells, the loss of CIC-7 or Ostm1 impairs lysosomal degradation of endocytosed proteins²¹. Similarly, *Drosophila* hemocytes lacking CIC-b are defective in the degradation of phagocytosed bacteria²². However, CIC-b and DmOstm1 were dispensable for dsRNA uptake, lysosomal targeting, and degradation in S2 cells (Fig. 3). Furthermore, although the late endosomes, known as multivesicular bodies (MVBs), are proposed to be sites regulating RISC activity^{23,24}, nuclear dsRNAs induced RNAi normally in hemocytes and eye pigment cells lacking CIC-b or DmOstm1 (Fig. 2). Thus, the loss of CIC-b or DmOstm1 does not generally affect lysosomal functions but rather specifically impedes the dsRNA-mediated LMP process for RNAi induction.

We showed that endocytosed dsRNAs exhibit an intrinsic ability to induce CIC-b/DmOstm1-dependent LMP for their cytosolic release (Fig. 5). As dsRNAs are highly negatively charged molecules, their accumulation in the lysosomes may lead to an influx of counter-ions,

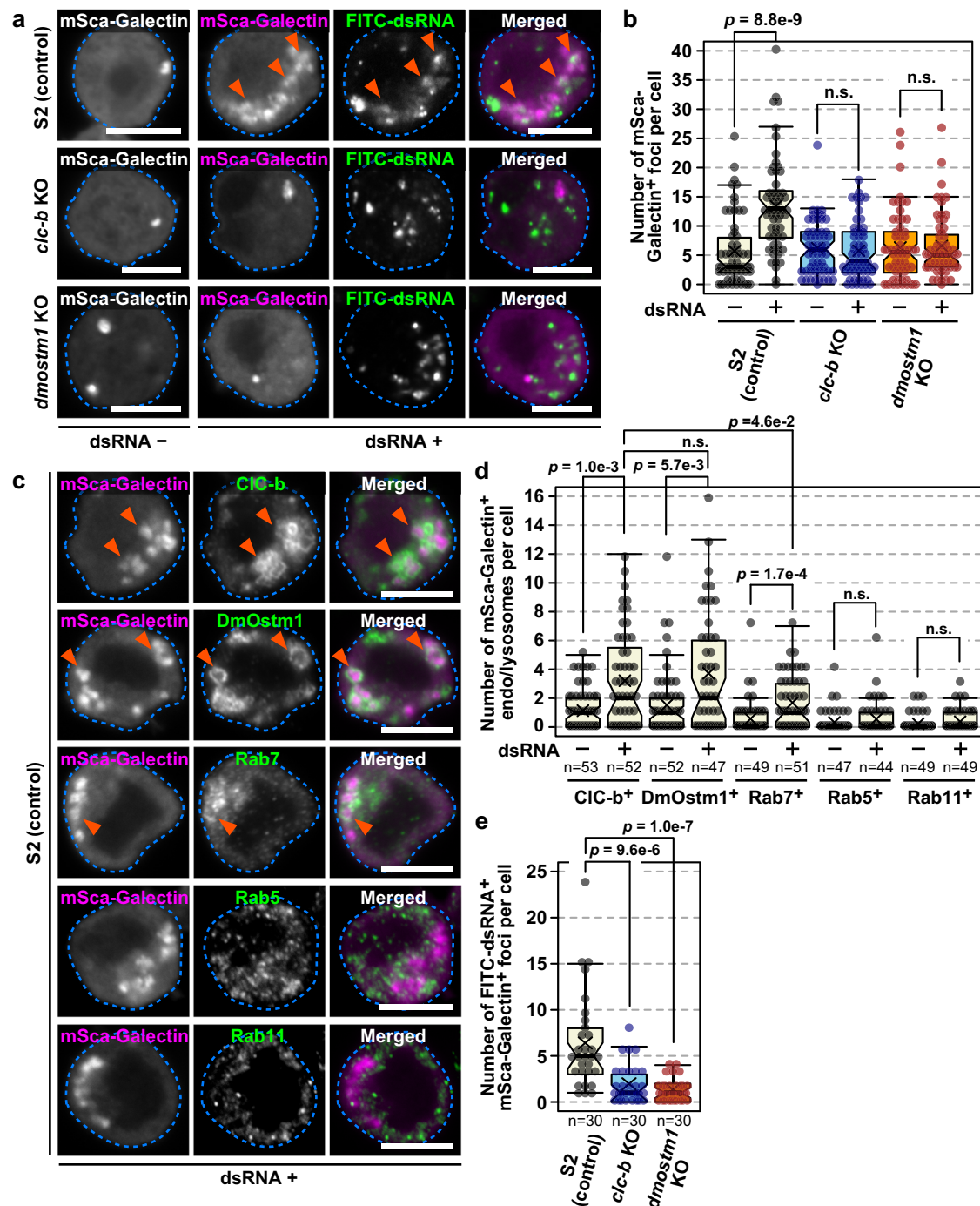


Fig. 5 | Endocytosed dsRNAs induce LMP in a CIC-b/DmOstm1-dependent manner. **a** Representative images of mSca-Galectin and FITC-dsRNAs in control, *clc-b*, and *dmostm1* KO S2 cells. Cells expressing mSca-Galectin were treated with or without 5 μ g/mL FITC-dsRNAs for 24 h. mSca-Galectin⁺ FITC-dsRNA⁺ foci are indicated with arrowheads. **b** The number of mSca-Galectin⁺ per mSca-Galectin-expressing cell treated with or without FITC-dsRNAs for 24 h. Sixty cells were counted in each condition. **c** Representative images of mSca-Galectin-expressing control S2 cells immunostained for endo/lysosomal proteins (CIC-b, DmOstm1, Rab7, Rab5, or Rab11). Cells were treated with 5 μ g/mL FITC-dsRNAs for 24 h. mSca-Galectin⁺ endo/lysosomal protein⁺ foci are indicated with arrowheads. **d** The number of double positive foci for mSca-Galectin and endo/lysosomal proteins

(CIC-b, DmOstm1, Rab7, Rab5, or Rab11) per mSca-Galectin-expressing cell treated with or without *dsfluc* for 24 h. The number of cells (*n*) examined is indicated in the graph. **e** The number of mSca-Galectin⁺ FITC-dsRNA⁺ foci per mSca-Galectin-expressing cell treated with FITC-dsRNAs for 24 h. The number of cells (*n*) examined is indicated in the graph. For **a** and **c**, cells are outlined by blue dashed lines. Scale bars: 5 μ m. For **b**, **d**, and **e** *p*-values were calculated using two-sided Mann–Whitney U test. n.s. not significant (*p* > 0.05). All box plots indicate the median (center line), the mean (\times), the interquartile range (IQR) between the first and third quartile (Q1 and Q3; box), 1.5 \times IQR above Q1 and below Q3 (whiskers), and each data point (dots). Statistics source data tested for Fig. 5 are provided in the Source Data file.

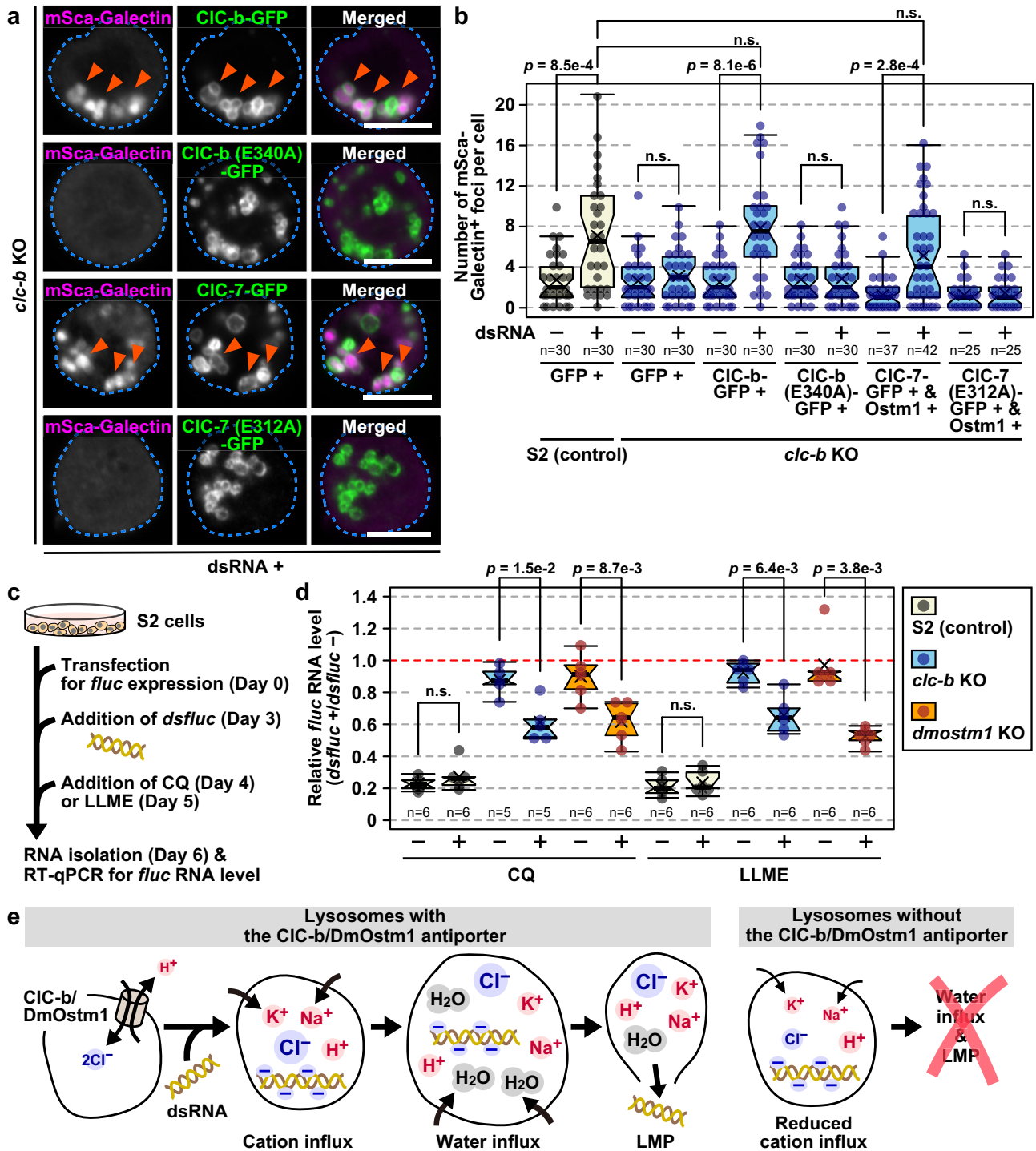


Fig. 6 | Pharmacological induction of LMP restores extracellular dsRNA-directed RNAi in *clc-b* or *dmostm1* KO cells. a Representative images of *clc-b* KO cells co-expressing mSca-Galectin and either wild-type or mutated CIC-b/CIC-7-GFP. Mouse CIC-7-GFP was co-expressed with mouse Ostm1 for its functions. Cells were treated with 5 μg/mL FITC-dsRNAs for 24 h. mSca-Galectin⁺ CIC-b/CIC-7-GFP⁺ foci are indicated with arrowheads. mSca-Galectin⁺ CIC-b/CIC-7-GFP⁺ foci are indicated with arrowheads. Cells are outlined by blue dashed lines. Scale bars: 5 μm. **b** The number of mSca-Galectin⁺ foci per mSca-Galectin-expressing cell treated with or without dsRNAs for 24 h. The number of cells (n) examined is indicated in the graph. **c** A schematic diagram of experiments to evaluate effects of LMP inducers (CQ and LLME) on the RNAi efficiency. **d** The relative *fluc* mRNA levels determined by RT-qPCR in *dsfluc*-treated control, *clc-b*, and *dmostm1* KO S2 cells that were transfected with *fluc*-expressing plasmids. For the CQ treatment, cells

cultured with or without *dsfluc* for 24 h were treated with or without 100 μM CQ for 48 h in the absence or presence of *dsfluc*. For the LLME treatment, cells cultured with or without *dsfluc* for 48 h were treated with or without 200 μM LLME for 24 h in the absence or presence of *dsfluc*. The number of independent experiments (n) is indicated in the graph. The *fluc* mRNA levels in *dsfluc*-untreated cells were arbitrarily defined as 1. **e** Schematic model for the dsRNA-mediated LMP process. See discussion for details. For **b** and **d**, *p*-values were calculated using two-sided Mann-Whitney U test. n.s. not significant (*p* > 0.05). All box plots indicate the median (center line), the mean (×), the interquartile range (IQR) between the first and third quartile (Q1 and Q3; box), 1.5× IQR above Q1 and below Q3 (whiskers), and each data point (dots). Statistics source data tested for Fig. 6 are provided in the Source Data file.

such as sodium and potassium ions, which are major lysosomal cations, to maintain electroneutrality. It is conceivable that the cation influx is followed by water influx because of an osmotic imbalance across the lysosomal membrane, resulting in lysosomal swelling and LMP (Fig. 6e). Given that the chloride ion is a prime lysosomal anion required to maintain ionic homeostasis and transmembrane potential²⁵, the chloride ion influx mediated by the CIC-b/DmOstm1 antiporter may provide the driving force for the counter-cation influx. Interestingly, the chloride ion concentration in the endo/lysosomes depends on the activity of the proton pump v-ATPase^{26,27}. Considering that the v-ATPase depletion causes the RNAi defect⁷, lysosomal acidification may contribute to dsRNA-mediated LMP.

RNAi regulates antiviral immunity in a wide range of organisms, including fungi, plants, invertebrates, and mammals^{28,29}. In *Drosophila*, DCV infection induces both cell-autonomous and non-autonomous RNAi responses, both of which affect susceptibility to virus infection¹⁰. In the cell-autonomous mode of antiviral response, the Dicer-2/R2D2 endonuclease complex processes dsRNAs derived from the replicating viral genome into siRNAs, which are subsequently loaded into the Ago2-RISCs for RNAi response in infected cells¹⁰. Interestingly, DCV is internalized into the cell via clathrin-mediated endocytosis and remodels the Golgi apparatus to form unique vesicular compartments³⁰. Because the viral RNA replication occurs on the surface of the remodeled compartment³⁰, viral dsRNA appears to be processed into siRNA independently of the lysosomal CIC-b/DmOstm1 activity as observed (Fig. 2f). In the cell non-autonomous mode, it has been reported that *Drosophila* hemocytes take up viral RNAs released through the lysis of infected cells via endocytosis and copy them into viral cDNAs, which serve as templates for de novo synthesis of virus-derived siRNAs^{11,12}. These siRNAs are incorporated into the extracellular vesicles, which spread to distal sites within the fly body and confer systemic antiviral RNAi¹². Given that extracellular vesicles enter the cells via endocytosis³¹, the lysosomal CIC-b/DmOstm1 antiporter may promote cytosolic translocation of endocytosed virus-derived siRNAs in extracellular vesicles for RNAi-associated systemic antiviral immunity.

Methods

Cells and reagents

Drosophila Kc and S2 cells derived from embryonic hemocyte lineages were cultured in Schneider's *Drosophila* medium (Thermo Fisher Scientific, Waltham, Massachusetts, United States of America) supplemented with 10% heat-inactivated fetal bovine serum (FBS) (Gemini Bio-Products, Woodland, California, USA) and antibiotics (100 U/mL penicillin and 100 µg/mL streptomycin) (Nacalai Tesque Inc., Kyoto, Japan) at 25 °C. For *clc-b* or *dmostm1* KO S2 cells, blasticidin (InvivoGen, San Diego, California, USA) was added to a final concentration of 25 µg/mL. HilyMax (Dojindo, Kumamoto, Japan) was used to transfect cells with plasmids. Bafilomycin A1 was purchased from LKT Laboratories Inc. (St. Paul, Minnesota, USA). LysoTracker Red DND-99 and dextran-tetramethylrhodamine (10,000 MW, lysine fixable) were purchased from Thermo Fisher Scientific. Chloroquine diphosphate was purchased from Fujifilm Wako Chemicals (Osaka, Japan). L-leucyl-L-leucine methyl ester monohydrochloride was purchased from Cayman Chemical (Ann Arbor, Michigan, USA).

Flies

Drosophila melanogaster stocks were reared on standard cornmeal and agar medium at 25 °C. The following strains were obtained from Bloomington stock center (Bloomington, Indiana, USA) and Kyoto stock center (Kyoto, Japan): *Hml-Gal4*, *UAS-2×EGFP* (BDSC #30140 on the 2nd chromosome and BDSC #30142 on the 3rd chromosome), *UAS-GFP.dsRNA* (BDSC #9331 on the 2nd chromosome and BDSC #9330 on the 3rd chromosome), *GMR-w.IR* (BDSC #32068), *Df(2R)BSC880* (BDSC #30585), *Df(3L)ED208* (BDSC #8059), *dcr-2^{LS1JfSX}* (BDSC

#33053), and *dcr-2^{AS00V}* (BDSC #32065), *ago2^{H4}* (DGRC #109027), *ago2⁶⁵⁴* (BDSC #36512).

Viruses

DCV virions were purified following a previously published protocol with minor modifications³². Briefly, S2 cells were inoculated with virions and cultured for five days. The cell culture supernatant was centrifuged to eliminate the cell debris, placed on a 10% sucrose/PBS cushion, and centrifuged at 84,600 × g for 3 h. The pellet was resuspended in PBS and filtered using a 0.45 µm pore size filter. The virion suspensions were aliquoted and stored at -80 °C for further analysis. Viral titers were measured by endpoint dilution assay on S2 cells and calculated as TCID50/mL according to the Reed–Muench method.

Plasmids

For *pAc-GFP*, *pAc-clc-b-GFP*, *pAc-lamp1-tdTom*, *pAc-clc-7-GFP*, *pAc-ostm1*, *pAc-mChe-dcr-2*, *pAc-mSca-R2D2*, and *pAc-mSca-galectin* (RE) plasmids, the PCR-amplified CDSs of each gene were digested with appropriate restriction enzymes, and the resultant fragments were inserted into the *pAc5.1/V5-HisA* vector (Invitrogen, Carlsbad, California, USA). *pAc-clc-b(E340A)-GFP* and *pAc-clc-7(E312A)-GFP* plasmids were generated via primer-mediated site-directed mutagenesis. Primers used for the plasmid construction are shown in Supplementary Table 2. The integrity of constructs was verified by DNA sequencing.

Antibodies

For anti-CIC-b antibodies, the CDSs for N-terminal CIC-b (amino acids 1-147) were inserted into the *pET-16b* vector (Novagen, Madison, Wisconsin, USA) to produce a 6×His-tagged protein (see Supplementary Table 2 for primer sets used for the plasmid construction). The fusion proteins were produced in *E. coli* BL21 strain using standard induction conditions and were purified using Ni-NTA agarose (Invitrogen). For anti-DmOstm1 antibodies, the CDSs for the cytosolic region of DmOstm1 (amino acids 220-315) were inserted into the *pProExHTa* vector (Gibco BRL, Gaithersburg, Maryland, USA) to produce a 6×His-tagged protein (see Supplementary Table 2 for primer sets used for the plasmid construction). The fusion proteins were expressed in *E. coli* BL21 and were purified using Ni-NTA agarose (Qiagen, Hilden, Germany) under denaturing conditions. The polyclonal antisera were raised in rabbits and rats by SCRUM Inc. (Tokyo, Japan).

dsRNAs

The templates for dsRNA synthesis were amplified by PCR using primers with the T7 promoter sequence (5'-TAATACGACTCACTATAGGG-3'). The PCR fragments for each gene were as follows: *clc-b* (nucleotides 392-829), *dmostm1* (nucleotides 123-542), *GFP* (nucleotides 230-716), and *fluc* (nucleotides 18-151, 18-276, 18-572, and 18-572). The primer sequences used for the templates for dsRNA synthesis are shown in Supplementary Table 3. The dsRNAs were synthesized using the HiScribe T7 High Yield RNA Synthesis Kit (New England Biolabs, Ipswich, Massachusetts, USA) according to the manufacturer's instructions. For the synthesis of FITC- or biotin-labeled dsRNAs, the partial UTP was replaced with FITC-UTP (Roche, Basel, Switzerland) or biotin-UTP (Roche), respectively. After in vitro transcription, the template DNA was digested by incubation with 1 U/µL RNase-free DNase I (Roche) at 37 °C for 45 min. The reaction mixture was then purified using NucleoSpin RNA Clean-up columns (Takara Bio Inc., Shiga, Japan). Purified RNAs were mixed with equal volume of 2× annealing buffer (10 mM Tris, pH 7.5, 50 mM NaCl, 1 mM EDTA) and were annealed by heating at 95 °C for 2 min and subsequent slow cooling to 25 °C at a rate of -1 °C/min in a thermal cycler. For target gene knockdown, 1.0 × 10⁶ cells were seeded in 2 mL of the serum-free medium containing 2 µg of dsRNAs per well in a 6-well plate and were incubated for 3 days.

clc-b and *dmostm1* KO S2 cell lines

For the generation of *clc-b* or *dmostm1* KO S2 cell lines, 1.7×10^6 S2 cells in a 6-well plate were co-transfected with two *pDCC6* plasmids expressing Cas9 and sgRNAs targeted to the 5' and 3' regions of the *clc-b* or *dmostm1* gene, and *pBlueScript-CoBlast* plasmids containing the blasticidin-resistance gene flanked by 1 kb arms homologous to upstream (5' arm) and downstream (3' arm) regions of the *clc-b* or *dmostm1* gene. Oligo pairs with sgRNA target sequences are shown in Supplementary Table 4. Following two days of incubation, transfected cells were seeded in a 24-well plate (2.5×10^5 cells per well) in the presence of 25 $\mu\text{g}/\text{mL}$ blasticidin and were incubated for 3–4 days at 25 °C. Blasticidin-resistant cells were then seeded at 1.0–1.5 cells per well of a 96-well plate in the presence of 25 $\mu\text{g}/\text{mL}$ blasticidin to isolate cell lines derived from single-cell clones. Because S2 cells cease proliferation when seeded at a low density³³, the transfected cells were co-cultured with 1×10^5 wild-type S2 cells per well, which gradually died out due to blasticidin treatment. After two weeks of incubation, cells from wells containing a single colony were seeded in a 24-well plate and were cultured to confluence. Clonal cells in 350–450 μL culture medium were lysed in 25 μL of lysis buffer (10 mM Tris, pH 8.0, 25 mM NaCl, 1 mM EDTA, 0.2 mg/mL proteinase K) for 60 min at 37 °C and then for 5 min at 95 °C to inactivate proteinase K. 1 μL of lysed cells was subjected to PCR analyzes using OneTaq DNA Polymerase (New England Biolabs) in a 20 μL reaction mixture with 200 μM dNTPs (New England Biolabs) and 0.2 μM primer pairs, in order to determine the replacement of the *clc-b* or *dmostm1* gene with the blasticidin-resistance gene. The primer pairs used were 5'-ATGCAAGC TGCTGTTCCGCTGG-3' and 5'-ATACGCCTAGAGCCACATACACC-3' for the *clc-b* gene region, or 5'-GTTCTAATTGTCCTGTCCGCTG-3' and 5'-CTACCTCAGGAACCAGTTGGAC-3' for the *dmostm1* gene region. PCR was performed on a GeneAmp PCR System 2700 or 2720 (Applied Biosystems, Carlsbad, California, USA) under the following cycling conditions: 94 °C for 30 s, 35 cycles of 94 °C for 30 s, 58 °C for 30 s, and 68 °C for 5 min (for *clc-b*) or 3 min (for *dmostm1*), followed by 68 °C for 5 min. 1 μL of PCR products in *dmostm1* samples were digested with 2 U *Bam*HI (New England Biolabs), which cut only amplicons generated from the *dmostm1* gene, but not from the blasticidin-resistance gene, in a 10 μL reaction mixture with 1 \times CutSmart Buffer (New England Biolabs). The undigested and digested PCR products were separated by electrophoresis on a 1% agarose gel. Because S2 cells are minimally tetraploid³⁴, the cell lines with the gene replacement were then subjected to quantitative PCR (qPCR) to evaluate the gene copy number. The mRNA level was also quantified by reverse transcription qPCR (RT-qPCR) (see Supplementary Table 5 for the primers), and protein expression was evaluated by immunofluorescence and western blotting analyzes to identify *clc-b* or *dmostm1* KO clones.

clc-b and *dmostm1* mutant flies

Mutants for *clc-b* and *dmostm1* were isolated using the CRISPR-Cas9 system as described previously³⁵. Oligonucleotides for the single guide RNA (sgRNA) were designed using the CRISPR Optimal Target Finder program³⁶ (<http://targetfinder.flycrispr.neuro.brown.edu/>), to target 20 to 110 nt downstream of the start codon of the *clc-b* and *dmostm1* loci (see Supplementary Table 4 for oligo pairs with sgRNA target sequences). The sgRNAs were ligated into the *pDCC6* vector³⁷ linearized with *Bbs* I. The plasmids were injected into *y w* eggs, and the resulting adults were crossed with balancer flies. CRISPR-Cas9-induced mutations in F1 males were detected through T7 endonuclease I assays³⁸ and direct sequencing of PCR products.

Injection of dsRNAs into flies

A glass needle of 20 μm luminal diameter was made by pulling a glass capillary tube (Drummond Scientific Company, Broomall, Pennsylvania, USA) using a P-97/IVF micropipette puller (Sutter Instrument Co., Novato, California, USA), with 1 mm of the tip clipped off to generate

an opening. The glass needle was connected to a rubber tube with a plastic mouthpiece and was back-filled with dsRNA solution (0.8 $\mu\text{g}/\mu\text{L}$ dsRNA/PBS) containing 0.01% Fast Green FCF dye (Waldeck GmbH & Co. KG, Münster, Germany), which was used as a visual tracer. ~200–250 nL (160–200 ng of dsRNAs) of the dsRNA solution per fly was injected by mouth pipetting into the abdominal cavity of 4- to 7-day-old adult female flies that were anaesthetized by CO₂. Injected flies were transferred to a new vial containing cornmeal and agar medium. A day after the injection, total RNA was isolated, and the expression level of *GFP* was determined by RT-qPCR.

Fly infection

Each fly strain was confirmed to be absent from *Wolbachia* bacteria by PCR analysis for amplification of the *Wolbachia* 16S rRNA gene because *Wolbachia* increases the resistance of *Drosophila* to RNA viruses³⁹. Three- to five-day-old adult female flies were intrathoracically injected with 70 nL of viral suspension (10^6 TCID₅₀/mL) per fly using Nanoject II (Drummond, Broomall, Pennsylvania, USA). ~20 flies were cultured in a fresh vial at 25 °C after injection and monitored daily for survival. Each assay was repeated more than 5 times to evaluate reproducibility, and more than 100 flies were examined per condition. The R software was used to draw Kaplan-Meier survival curves and to evaluate differences in survival curves by the log-rank test. For viral RNA loads, total RNA was isolated from 5 DCV-injected adult flies with TRIzol (Thermo Fisher Scientific) according to the manufacturer's instructions. Fifteen individuals were used per data point. 1 μg of the total RNA was reverse-transcribed using random primers (Promega) and ReverTra Ace (TOYOBO, Osaka, Japan). RT-qPCR was performed using FastStart Essential DNA Green Master (Roche) in a 20 μL volume with 5 μL of cDNA, using primers described by Sansone et al.⁴⁰; Supplementary Table 5. The DCV RNA levels were normalized to the *rp49* mRNA levels.

RT-qPCR

For RT-qPCR to evaluate the gene copy number, S2 cells in 350–450 μL culture medium in 24-well plates were lysed in 25 μL of lysis buffer (10 mM Tris, pH 8.0, 25 mM NaCl, 1 mM EDTA, 0.2 mg/mL proteinase K) for 60 min at 37 °C and then for 5 min at 95 °C to inactivate proteinase K. 2 μL of 1:32 diluted lysed cells was used for RT-qPCR using Luna qPCR master mix (New England Biolabs) in a 10 μL reaction mixture with 0.25 μM primer pairs listed in Supplementary Table 5. RT-qPCR was performed on a Step One Plus real-time PCR system (Applied Biosystems) under the following cycling conditions: 95 °C for 1 min, 40 cycles of 95 °C for 5 s and 60 °C for 30 s. Standard curves were generated using 1:4 serial dilutions of mixed test samples over a range of 1:2–1:512. Gene levels of *clc-b* or *dmostm1* were normalized to *rp49* gene levels.

For RT-qPCR to evaluate the mRNA level, ~10 adult flies or 5×10^6 S2 cells were, respectively, lysed in 500 μL or 300 μL of Isogen II (Nippon Gene Co., Ltd., Toyama, Japan). The total RNA was extracted according to the manufacturer's instructions. Yield and purity were determined photometrically. The cDNA was prepared using Luna-Script RT SuperMix (New England Biolabs) in a 10 μL reaction mixture containing 0.5 μg of the total RNA. RT-qPCR was performed as described above in a 10 μL volume with 2 μL of 1:32 diluted cDNA. The *GFP* mRNA levels in adult flies expressing *GFP* under the control of a hemocyte-specific driver *Hml* Gal4 were normalized to the *hml* mRNA levels. The *fluc* mRNA levels in S2 cells co-transfected with *fluc*- and *Renilla luciferase* (*Rluc*)-expressing plasmids were normalized to the *Rluc* mRNA levels. Data were analyzed using the StepOne Software v2.2.2. RT-qPCR analysis was performed using four to six independent samples in two technical replicates.

Electrophoresis and detection of biotin-RNAs

The total RNA was isolated using Isogen II (Nippon Gene Co., Ltd.) from cells that were seeded at 1×10^6 cells per well of a 6-well plate and

treated with biotin-RNA for 24 h. The loading sample was prepared by mixing equal volumes of RNA solution and 2× loading buffer (98% formamide, 5 mM EDTA [pH 8.0], 0.05% bromophenol blue, 0.05% xylene cyanol) and was subjected to electrophoresis on 15% acrylamide gel containing 1× TBE and 7 M urea. The separated RNAs were then transferred to a nylon membrane (GeneScreen Plus, NEN Life Science Products Inc., Boston, Massachusetts, USA) and were cross-linked with a CL-1000 UV Crosslinker (UVP, Upland, California, USA) using an energy setting of 120,000 μJ/cm². The membrane was incubated with streptavidin-HRP (Thermo Fisher Scientific), followed by incubation with SuperSignal West Femto (Thermo Fisher Scientific). Chemiluminescent signals were detected with a LAS-3000 Mini image analyzer (Fujifilm, Tokyo, Japan).

Immunoprecipitation and immunoblot analysis

Co-immunoprecipitation experiments for CIC-b and DmOstm1 were performed according to procedures reported by Schrecker et al.¹³, with some modifications. 5×10^7 of S2 or *dmostm1* KO cells were washed once with PBS and cell pellets were flash-frozen in liquid nitrogen. The thawed cell pellets were lysed in 1 mL of Co-IP buffer [2% lauryl maltose neopentyl glycol (LMNG; Anatrace, Maumee, Ohio, USA), 20 mM HEPES pH 7.5, 150 mM KCl] supplemented with Protease Inhibitor Cocktail (Nacalai Tesque Inc.) for 1 h at 4 °C with gentle rotation. The lysates were cleared by centrifugation at 16,000 × *g* for 15 min at 4 °C, and the total protein concentrations of the supernatants were determined using the BCA Protein Assay (Thermo Fisher Scientific), using bovine serum albumin as a standard. The protein concentration of cleared lysates was adjusted to 2 mg/mL with Co-IP buffer. Five microliters of rat anti-DmOstm1 or pre-immune sera were incubated with Dynabeads Protein G magnetic beads (Thermo Fisher Scientific) in PBS containing 0.2% Tween 20 (PBST) for 2 h at room temperature and washed twice with PBST. The pre-immune or anti-DmOstm1 antibody-immobilized beads were incubated with 500 μL (1 mg of total protein) of S2 or *dmostm1* KO cell lysates for 1 h at 4 °C with gentle rotation. The beads were then washed five times with 900 μL of wash buffer (0.1% LMNG, 50 mM Tris-HCl pH 8.0, 150 mM KCl, 2 mM DTT). Bound proteins were eluted from the beads by incubation with 50 μL of 2× NuPAGE LDS Sample Buffer containing 200 mM DTT for 10 min at 70 °C. The eluted proteins were separated on 4–12% mPAGE gels with MOPS buffer (Millipore, MA, USA) and were transferred to Immobilon-P membranes (Millipore). The membranes were subjected to western blot analysis using rabbit anti-CIC-b (1:1,000) or rabbit anti-DmOstm1 (1:4,000), followed by the HRP conjugated secondary antibodies (Jackson ImmunoResearch Laboratories Inc., West Grove, Pennsylvania, USA; 1:50,000). The membranes were then incubated with ChemiLumi One Super (Nacalai Tesque Inc.), and the chemiluminescent signals were detected with the LAS-3000 Mini image analyzer (Fujifilm, Tokyo, Japan).

Small RNA-seq analysis

1×10^6 of S2, *clc-b*-KO, or *dmostm1*-KO cells were treated with dsRNA as described⁴¹. Cells were cultured in 1 mL of serum-free Schneider's medium with or without 15 μg of *fluc* dsRNA (nt 18–572) in a 6-well plate at 25 °C for 30 min. Subsequently, 2 mL of Schneider's medium supplemented with 10% FBS was added and cultured at 25 °C for 40 hr. Cells were harvested and washed with PBS twice. Cell pellets were stored at –80 °C. DCV- or control saline-injected female flies were harvested at the same time from the DCV injection and RNA quantification experiments. Ten flies for each genotype were cultured for 24 h and stored at –80 °C. The Ago2-containing complex was immunopurified as described¹⁸. Briefly, flies or cells were homogenized in 500 μL of PBS supplemented with 1 mM EDTA, 0.1 mM DTT, 1% Empigen (Sigma), and protease inhibitors (Nacalai Tesque Inc.). The homogenized lysates were incubated on ice for 1 h. Lysates were centrifuged at 16,000 × *g* for 10 min at 4 °C, and supernatants were

incubated with anti-Ago2 antibody immobilized Dynabeads Protein G for 3 h at 4 °C with gentle rotation. Beads were washed with the same buffer five times and extracted with Isogen II (Nippon Gene Co., Ltd.). Purified RNA samples were subjected to small RNA library construction using NEBNext Multiplex Small RNA Library Prep Set for Illumina (New England Biolabs Inc, MA, USA). To prevent the contamination of 2 S rRNA-derived sequence in the library, a 2 S block oligonucleotide (5'-TACAACCCTCAACCATATGTAGTCCAAGCA/3SpC3/-3') was added during the 5'-adapter ligation step⁴². Single-end, 75-bp sequencing of the library was conducted using NextSeq500 (Illumina, CA, USA). Small RNA sequences of 21 bases were matched to the *Drosophila* C virus genome (isolate G) or the firefly luciferase coding sequence from pGL3 plasmid (Promega, WI, USA) using Bowtie v1.3.1 (<https://bowtie-bio.sourceforge.net/index.shtml>). Unmatched reads were then mapped to the *Drosophila* transposons [Berkeley *Drosophila* Genome Project (BDGP) release 6.48] and genomic sequence without transposons (BDGP release 6.32) using Bowtie v1.3.1.

Immunofluorescent staining

5×10^5 S2 cells plated on a poly-L-lysine-coated circular coverslip (12 mm diameter) in wells of 24-well plates were fixed in 4% paraformaldehyde (PFA)/PBS for 20 min and washed with PBS three times. Fixed cells were permeabilized with 0.1% Triton X-100/PBS for 5 min at room temperature. After a rinse with PBS and subsequent incubation with blocking buffer (2% BSA/0.005% Tween 20/PBS) for 30 min at room temperature, coverslips were incubated with primary antibodies diluted in blocking buffer for 1 h at room temperature and washed three times with 0.005% Tween 20/PBS for 5 min each. The primary antibodies used in this study were rabbit anti-CIC-b (1:1000), rat anti-DmOstm1 (1:1,000), guinea pig anti-Rab5⁽⁴³⁾ (1:5,000), affinity purified rabbit anti-Rab7⁽⁴⁴⁾ (1:2,000), affinity purified rabbit anti-Rab11⁽⁴⁴⁾ (1:8,000). Coverslips were then incubated with Alexa-conjugated secondary antibodies (Invitrogen; 1:500) and 1 μg/mL 4',6-diamidino-2-phenylindole, dihydrochloride (DAPI) diluted in blocking buffer for 1 h at room temperature and washed three times with 0.005% Tween 20/PBS for 5 min each. The coverslips were mounted on slides using ProLong Diamond (Thermo Fisher Scientific). All fluorescence images were acquired by scanning in sequential mode on a Leica TCS SP8 confocal microscope with a 100× NA 1.46 oil immersion lens (Leica, Wetzlar, Germany). Images were processed with Adobe Photoshop (Adobe Systems Incorporated, San Jose, California, USA).

LysoTracker staining

1×10^6 cells per well were seeded on coverslips placed in a 24-well culture plate and incubated with 100 nM LysoTracker Red DND-99 for 1 h at 25 °C. For BafA1 treatment, cells were cultured with 200 nM BafA1 for 4 h at 25 °C prior to LysoTracker staining. Cells stained with LysoTracker were then fixed in 4% PFA/PBS.

Image analyzes

For co-localization analyses, Pearson's coefficients for regions of interest (ROIs) in background-subtracted images were calculated using the Coloc 2 plugin in Fiji software⁴⁵ (<https://imagej.net/Fiji>) with preset parameters. For quantification of FITC-dsRNA signals, z-section images (spaced by 1.5 μm over 6–9 μm) were acquired using a Leica TCS SP8 confocal microscope with a 100× NA 1.46 oil immersion lens (Leica) in the photon-counting mode of the HyD detector. The signal intensity of each z-section was measured by Fiji software. The sum of intensities from multiple z-sections was assumed to be the total FITC intensity per cell. Significant differences (p) were calculated using the two-sided Mann–Whitney U test.

Statistics and reproducibility

The exact numbers of repetitions, cells, and flies tested for each experiment are indicated in the Source Data file. All experiments were

performed as two or more independent experiments. The same conclusions were obtained from each experiment. Data visualization and statistical tests were carried out using the R software. All box plots indicate the median (center line), the mean (\times), the interquartile range (IQR) between the first and third quartile (Q1 and Q3; box), $1.5 \times$ IQR above Q1 and below Q3 (whiskers), and each data point (dots). All bar graphs indicate the mean \pm SD (error bars) and each data point (dots). All p values were calculated using the two-sided Mann–Whitney U test, except for the Kaplan–Meier survival curves which were compared using the nonparametric log-rank test. A p -value less than 0.05 was considered significant. All exact p -values are provided in the Source Data file.

Reporting summary

Further information on research design is available in the Nature Portfolio Reporting Summary linked to this article.

Data availability

All data supporting the findings of this study are available in the article and its supplementary information. The raw datasets for all graphs and the uncropped images of the immunoblots presented in this study are provided as a Source Data file. The raw small RNA-sequencing data have been deposited in the NCBI Gene Expression Omnibus (GEO) database under accession number [GSE244523](https://www.ncbi.nlm.nih.gov/geo/query/acc.cgi?acc=GSE244523). Source data are provided in this paper.

References

- Tomari, Y. & Zamore, P. D. Perspective: machines for RNAi. *Genes Dev* **19**, 517–529 (2005).
- Huvenne, H. & Smagghe, G. Mechanisms of dsRNA uptake in insects and potential of RNAi for pest control: a review. *J. Insect Physiol.* **56**, 227–235 (2010).
- Mehlhorn, S., Hunnekuhl, V. S., Geibel, S., Nauen, R. & Bucher, G. Establishing RNAi for basic research and pest control and identification of the most efficient target genes for pest control: a brief guide. *Front. Zool.* **18**, 60 (2021).
- Nguyen, T. A. et al. SIDT2 transports extracellular dsRNA into the cytoplasm for innate immune recognition. *Immunity* **47**, 498–509.e6 (2017).
- Nguyen, T. A. et al. SIDT1 localizes to endolysosomes and mediates double-stranded RNA transport into the cytoplasm. *J. Immunol.* **202**, 3483–3492 (2019).
- Sopko, R. et al. A systems-level interrogation identifies regulators of *Drosophila* blood cell number and survival. *PLoS Genet.* **11**, e1005056 (2015).
- Saleh, M. C. et al. The endocytic pathway mediates cell entry of dsRNA to induce RNAi silencing. *Nat. Cell Biol.* **8**, 793–802 (2006).
- Jentsch, T. J. & Pusch, M. CLC chloride channels and transporters: structure, function, physiology, and disease. *Physiol. Rev.* **98**, 1493–1590 (2018).
- Lange, P. F., Wartosch, L., Jentsch, T. J. & Fuhrmann, J. C. ClC-7 requires Ostm1 as a beta-subunit to support bone resorption and lysosomal function. *Nature* **440**, 220–223 (2006).
- Kingsolver, M. B., Huang, Z. & Hardy, R. W. Insect antiviral innate immunity: pathways, effectors, and connections. *J. Mol. Biol.* **425**, 4921–4936 (2013).
- Saleh, M. C. et al. Antiviral immunity in *Drosophila* requires systemic RNA interference spread. *Nature* **458**, 346–350 (2009).
- Tassetto, M., Kunitomi, M. & Andino, R. Circulating immune cells mediate a systemic RNAi-based adaptive antiviral response in *Drosophila*. *Cell* **169**, 314–325 (2017).
- Gammon, D. B. & Mello, C. C. RNA interference-mediated antiviral defense in insects. *Curr. Opin. Insect Sci.* **8**, 111–120 (2015).
- Schrecker, M., Korobenko, J. & Hite, R. K. Cryo-EM structure of the lysosomal chloride-proton exchanger CLC-7 in complex with OSTM1. *eLife* **9**, e59555 (2020).
- Lee, Y. S. et al. Distinct roles for *Drosophila* Dicer-1 and Dicer-2 in the siRNA/miRNA silencing pathways. *Cell* **117**, 69–81 (2004).
- Kim, K., Lee, Y. S. & Carthew, R. W. Conversion of pre-RISC to holo-RISC by Ago2 during assembly of RNAi complexes. *RNA* **13**, 22–29 (2007).
- Nishida, K. M. et al. Roles of R2D2, a cytoplasmic D2 body component, in the endogenous siRNA pathway in *Drosophila*. *Mol. Cell* **49**, 680–691 (2013).
- Kawamura, Y. et al. *Drosophila* endogenous small RNAs bind to Argonaute 2 in somatic cells. *Nature* **453**, 793–797 (2008).
- Wang, F., Gómez-Sintes, R. & Boya, P. Lysosomal membrane permeabilization and cell death. *Traffic* **19**, 918–931 (2018).
- Weinert, S. et al. Transport activity and presence of CLC-7/Ostm1 complex account for different cellular functions. *EMBO Rep* **15**, 784–791 (2014).
- Wartosch, L., Fuhrmann, J. C., Schweizer, M., Stauber, T. & Jentsch, T. J. Lysosomal degradation of endocytosed proteins depends on the chloride transport protein CLC-7. *FASEB J* **23**, 4056–4068 (2009).
- Wong, C. O. et al. Lysosomal degradation is required for sustained phagocytosis of bacteria by macrophages. *Cell Host Microbe* **21**, 719–730 (2017).
- Gibbings, D. J., Ciaudo, C., Erhardt, M. & Voinnet, O. Multivesicular bodies associate with components of miRNA effector complexes and modulate miRNA activity. *Nat. Cell Biol.* **11**, 1143–1149 (2009).
- Lee, Y. S. et al. Silencing by small RNAs is linked to endosomal trafficking. *Nat. Cell Biol.* **11**, 1150–1156 (2009).
- Li, P., Gu, M. & Xu, H. Lysosomal ion channels as decoders of cellular signals. *Trends Biochem. Sci.* **44**, 110–124 (2019).
- Sonawane, N. D., Thiagarajah, J. R. & Verkman, A. S. Chloride concentration in endosomes measured using a ratioable fluorescent Cl⁻ indicator: evidence for chloride accumulation during acidification. *J. Biol. Chem.* **277**, 5506–5513 (2002).
- Chakraborty, K., Leung, K. & Krishnan, Y. High luminal chloride in the lysosome is critical for lysosome function. *eLife* **6**, e28862 (2017).
- Ding, S. W. & Voinnet, O. Antiviral immunity directed by small RNAs. *Cell* **130**, 413–426 (2007).
- Maillard, P. V., van der Veen, A. G., Poirier, E. Z. & Reis e Sousa, C. Slicing and dicing viruses: antiviral RNA interference in mammals. *EMBO J* **38**, e100941 (2019).
- Cherry, S. et al. 2006. COPI activity coupled with fatty acid biosynthesis is required for viral replication. *PLOS Pathog* **2**, e102 (2006).
- O'Brien, K., Breyne, K., Ughetto, S., Laurent, L. C. & Breakefield, X. O. RNA delivery by extracellular vesicles in mammalian cells and its applications. *Nat. Rev. Mol. Cell Biol.* **21**, 585–606 (2020).
- Merkling, S. H. & van Rij, R. P. Analysis of resistance and tolerance to virus infection in *Drosophila*. *Nat. Protoc.* **10**, 1084–1097 (2015).
- Zitzmann, J. et al. Single-cell cloning enables the selection of more productive *Drosophila melanogaster* S2 cells for recombinant protein expression. *Biotechnol. Rep. (Amst)* **19**, e00272 (2018).
- Lee, H. et al. DNA copy number evolution in *Drosophila* cell lines. *Genome Biol.* **15**, R70 (2014).
- Kina, H., Yoshitani, T., Hanyu-Nakamura, K. & Nakamura, A. Rapid and efficient generation of GFP-knocked-in *Drosophila* by the CRISPR-Cas9-mediated genome editing. *Dev. Growth Differ.* **61**, 265–275 (2019).
- Gratz, S. J. et al. Highly specific and efficient CRISPR/Cas9-catalyzed homology-directed repair in *Drosophila*. *Genetics* **196**, 961–971 (2014).

37. Gokcezade, J., Sienski, G. & Duchek, P. Efficient CRISPR/Cas9 plasmids for rapid and versatile genome editing in *Drosophila*. *G3 (Bethesda)* **4**, 2279–2282 (2014).
 38. Zhang, X., Ferreira, I. R. & Schnorrer, F. A simple TALEN-based protocol for efficient genome-editing in *Drosophila*. *Methods* **69**, 32–37 (2014).
 39. Teixeira, L., Ferreira, A. & Ashburner, M. The bacterial symbiont *Wolbachia* induces resistance to RNA viral infections in *Drosophila melanogaster*. *PLoS Biol.* **6**, e2 (2008).
 40. Sansone, C. L. et al. Microbiota-dependent priming of antiviral intestinal immunity in *Drosophila*. *Cell Host Microbe* **18**, 571–581 (2015).
 41. Li, C. & Zamore, P. D. RNAi in *Drosophila* S2 cells by dsRNA soaking. *Cold Spring Harb Protoc.* <https://doi.org/10.1101/pdb.prot097477> (2019).
 42. Fowler, E. K., Mohorianu, I., Smith, D. T., Dalmay, T. & Chapman, T. Small RNA populations revealed by blocking rRNA fragments in *Drosophila melanogaster* reproductive tissues. *PLOS One* **13**, e0191966 (2018).
 43. Tanaka, T., Tani, N. & Nakamura, A. Receptor-mediated yolk uptake is required for *oskar* mRNA localization and cortical anchorage of germ plasm components in the *Drosophila* oocyte. *PLoS Biol.* **19**, e3001183 (2021).
 44. Tanaka, T. & Nakamura, A. The endocytic pathway acts downstream of *Oskar* in *Drosophila* germ plasm assembly. *Development* **135**, 1107–1117 (2008).
 45. Schindelin, J. et al. Fiji: an open-source platform for biological-image analysis. *Nat. Methods.* **9**, 676–682 (2012).
- M.O., M.Y., K.H.N., and A.N. analyzed the data. T.T., T.Y., S.U., Y.S., K.M., M.O., M.Y., K.H.N., and A.N. organized all figures. T.T., N.T.S., K.B., and A.N. supervised the project. T.T., T.Y., and A.N. wrote the paper.

Competing interests

The authors declare no competing interests.

Additional information

Supplementary information The online version contains supplementary material available at <https://doi.org/10.1038/s41467-024-51343-4>.

Correspondence and requests for materials should be addressed to Akira Nakamura.

Peer review information *Nature Communications* thanks Bin Liu and the other anonymous reviewer(s) for their contribution to the peer review of this work. A peer review file is available.

Reprints and permissions information is available at <http://www.nature.com/reprints>

Publisher's note Springer Nature remains neutral with regard to jurisdictional claims in published maps and institutional affiliations.

Open Access This article is licensed under a Creative Commons Attribution-NonCommercial-NoDerivatives 4.0 International License, which permits any non-commercial use, sharing, distribution and reproduction in any medium or format, as long as you give appropriate credit to the original author(s) and the source, provide a link to the Creative Commons licence, and indicate if you modified the licensed material. You do not have permission under this licence to share adapted material derived from this article or parts of it. The images or other third party material in this article are included in the article's Creative Commons licence, unless indicated otherwise in a credit line to the material. If material is not included in the article's Creative Commons licence and your intended use is not permitted by statutory regulation or exceeds the permitted use, you will need to obtain permission directly from the copyright holder. To view a copy of this licence, visit <http://creativecommons.org/licenses/by-nc-nd/4.0/>.

© The Author(s) 2024

Acknowledgements

We thank the Bloomington *Drosophila* Stock Center for fly stocks; Addgene for the *pDCC6* plasmid; Drs. M. C. Siomi, H. Siomi, and K. Saito for anti-Ago2 antibody; and R. Iemura for laboratory assistance. This study was supported by the JSPS KAKENHI (Grant Number 22H02759 to T.Y., 21H04803 to N.T.S and 23H00364, 21H02489, and 17H03686 to A.N.), the program of the Inter-University Research Network for High Depth Omics, IMEG, Kumamoto University (to T.T. and A.N.), MEXT Promotion of Development of a Joint Usage/Research System Project: Coalition of Universities for Research Excellence Program (CURE) Grant Number JPMXP1323015486 (to A.N.), and research grants from Takeda Science Foundation and Mitsubishi Foundation (to A.N.).

Author contributions

T.T. and A.N. conceived the project and designed the study. T.T., T.Y., S.U., Y.S., and A.N. performed the experiments. T.T., T.Y., S.U., Y.S., K.M.,